

## Enhanced ionic conductivity and suppressed electronic conductivity of an Al- and Mn-added ceria solid electrolyte

Ji Young Park\*

Department of Materials Science and Engineering, University of Seoul, Seoul 02504, Korea

Gd-doped ceria (GDC) is a promising solid electrolyte for intermediate temperature solid oxide fuel cells (IT-SOFCs) due to its high oxygen-ion conductivity. However, commercialization is limited due to high grain boundary resistance and electronic conduction in reduced conditions. In this work, Al- and Mn-added GDCs were designed to overcome their weaknesses. GDC and Al- and Mn-added GDC powders were prepared using spray pyrolysis and then sintered using spark plasma sintering technique to obtain dense ceramic pellets. Additives enhanced the sinterability of the ceria leading to an increase in ionic conduction. More importantly, electronic conduction in GDC with the additives was suppressed under reduced conditions. This demonstrates that Al- and Mn-added GDC is a possible candidate as a solid electrolyte for IT-SOFCs.

**Keywords :** GDC, Additives, Ionic conduction, Electronic conduction.

### Introduction

SOFCs (Solid oxide fuel cells) electrochemically generate power in an environmentally friendly and efficient way by directly converting the chemical energy of fuel gas into electric energy [1-3]. Compared to other types of fuel cells, SOFCs use relatively inexpensive materials, have a relatively high tolerance to fuel impurities, enable hybrid operation, and have high efficiency. However, SOFCs operate at a high temperature ( $> 700$  °C), and therefore high temperature alloys or expensive ceramic materials that can withstand high temperature conditions are used in SOFCs [4-6]. Additionally, due to high temperature operation, the durability of materials used in the manufacture of SOFCs degrades; therefore, many studies have been conducted on fuel cells that operate at low temperatures. The operating temperature of a SOFC depends greatly on the properties of the solid electrolyte used [7-10].

Doped ceria, which has higher oxygen-ion conductivity than that of doped zirconia has been intensively studied to replace doped zirconia, a popular solid electrolyte [8-11]. However, it is known that the reduction reaction is caused under low oxygen partial pressure ( $P_{O_2}$ ) condition (fuel condition in fuel cells) and causes the problem of electron conduction [12, 13]. An equilibrium potential (open circuit voltage, OCV) associated with power output, is a function of the ionic transference number ( $t_i = s_{ion}/(s_{ion} + s_{electron})$ ),  $OCV = t_i C \ln(P_1/P_2)$  where  $C$  is a temperature-dependent constant, and  $P_1$  and  $P_2$

oxygen partial pressure on cathode and anode sides). When the electronic conductivity is substantially lower than the ionic conductivity,  $t_i$  is 1; while high electronic conductivity leads to  $t_i < 1$ , and OCV decreases; this reduction in OCV degrades the power output of the fuel cell. In addition to electronic conduction in a reducing environment, many cracks are generated due to lattice expansion by  $Ce^{4+} \rightarrow Ce^{3+}$  [14]. Such a mechanical weakness in reducing conditions has also prevented its commercialization as a solid electrolyte for SOFCs. Therefore, it is necessary to develop doped ceria with high  $t_i$  and mechanical stability (note that electronic conduction is related to mechanical properties in reduced conditions because the electronic charge carrier is produced by  $Ce^{4+} \rightarrow Ce^{3+}$ ).

In this study, we have produced Al- and Mn-added ceria with high  $t_i$ . Ceria powders were synthesized using ultrasonic spray pyrolysis (USP), a simple method for synthesizing multi-component materials, and the samples were quickly sintered using spark plasma sintering (SPS).

### Experimental

The preparation of a starting precursor solution to synthesize  $Gd_{0.8}Ce_{0.2}O_2$  (GDC) powders was carried out by mixing gadolinium nitrate ( $Gd(NO_3)_3 \times 9H_2O$ , Aldrich, 99.9%), cerium nitrate ( $Ce(NO_3)_2 \times 6H_2O$ , 99%, Aldrich), ethylene glycol (Reagent plus,  $> 99\%$ , Aldrich) and citric acid (Citric acid monohydrate, 99.5%, Daejung Chemical. Co.) in pure water. The concentration was fixed at 0.1 M. The solution for GDC- $Al_2O_3$ - $Mn_2O_3$  (GDCAM, GDC :  $Al_2O_3$  :  $Mn_2O_3$  = 97 vol % : 2 vol % : 1 vol %) nano-powder was mixed in the same manner. Aluminum nitrate ( $Al(NO_3)_3 \times 9H_2O$ , Alfa, 98%) and

\*Corresponding author:  
Tel : +82-2-6490-2400  
Fax: +82-2-6490-2404  
E-mail: tojyp19@uos.ac.kr

manganese nitrate ( $\text{Mn}(\text{NO}_3)_2 \times 6\text{H}_2\text{O}$ , Kanto, 98%) were added to the starting solution for GDC to prepare GDCAM. The solution mists were generated at a frequency of 1.6 MHz in an ultrasonic atomizer with transducer operation and were carried into a furnace preheated at a given temperature (900 °C). After the powder was collected, the spark plasma sintering technique was carried out to make high-density pellets of GDC and GDCAM. Each powder was filled with a cylindrical graphite die of 5 mm radius, heated to 1400 °C at a rate of 100 °C/min while a pressure of 80 MPa was applied, and sintered for 5 min.

The crystal structure of the as-synthesized powders and sintered pellets was characterized by X-ray diffractometer (XRD, Rigaku, D-2500). The morphology and microstructures of nanopowders were characterized by field emission scanning electron microscopy (FE-SEM, Hitachi S-4800). The distribution of elements was detected using energy dispersive X-ray analysis spectroscopy (EDS).

The relative density of the sintered samples was determined by the Archimedes method. Bending strength tests for the sintered samples were also conducted. For electrical measurements, platinum ink was painted on either side of the pellet and heated at 800 °C for 2 h to act as an electrode as well as an electric current collector. The electrical resistance was measured using two-probe ac techniques as a function of temperature under air and reducing atmosphere (5 %  $\text{H}_2/\text{N}_2$ -balance). In order to ensure sufficiently fast oxygen exchange at the interface of the sample, resistance was measured twice with increasing and decreasing temperature in the temperature range of 230-550 °C at a fixed  $\text{P}_{\text{O}_2}$ . For the reducing environment test, the temperature was swept two times in a range of 230-550 °C. The first experiment was conducted within 12 h under reducing condition (short-term test where the swept temperature was 230 °C  $\rightarrow$  550 °C  $\rightarrow$  230 °C). In the second-time experiment, the resistance of the specimen already exposed under the reducing environment for 12 h was measured again

in the same environment for 12 h (long-term test where the swept temperature was 230 °C  $\rightarrow$  550 °C  $\rightarrow$  230 °C). As another test, resistance was examined as a function of time under the reducing condition (5 %  $\text{H}_2/\text{N}_2$ -balance gas was used) to determine whether the Al- and Mn- added sample prevents electronic conduction in a reduced atmosphere.

AC impedance spectra were obtained in the frequency range of 1 Hz to 10 MHz using an impedance analyzer (Material Mates 7260), and the Z-view program (Scribner Associates) was used for the fitting of data.

## Results and Discussion

The solid state reaction, precipitation and sol-gel methods are representative ceramic processing techniques used for the synthesis of solid electrolytes of SOFCs [15, 16]. However, it is difficult to achieve optimal powder characteristics for multi-component materials with these methods, because the materials must be subjected to subsequent calcination and mixing steps. Moreover, the multi-component materials obtained by such methods can be unintentionally agglomerated without even distribution; these phenomena deteriorate as particle sizes decrease to nanoscale. By implementing USP, a simple and versatile synthetic method, GDC powders were obtained.

Fig. 1 shows the XRD patterns of (a) as-synthesized powders and (b) sintered pellets of GDC and GDCAM. As seen, the detected peaks for both cases were matched with JCPDS peaks of  $\text{CeO}_2$ , indicating that the desired fluorite cubic-crystal structure (space group :  $\text{Fm}\bar{3}\text{m}$ ) was well formed. However, the peaks of as-synthesized powders are not sharp but broad. This peak broadening is attributed to the nano crystal size of the powder,  $\sim 10$  nm, which was calculated from Sherrer's equation with the broadening. Additional peaks detected in the sintered pellet of GDCAM were  $\text{GdAlO}_3$ , which is a well-known secondary phase formed in ceria and alumina composites [17].

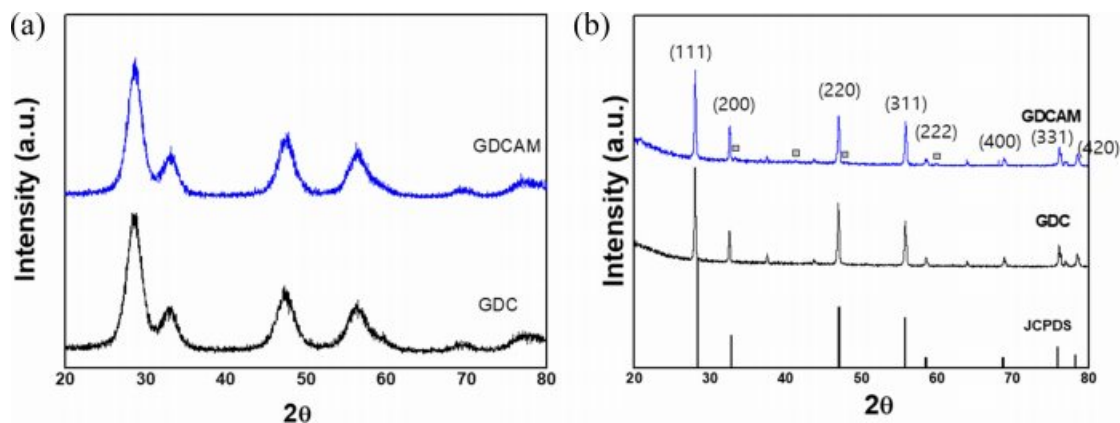


**Fig. 1.** X-ray diffraction patterns of GDC and GDCAM (a) powders and (b) sintered pellets. In Fig. 1b, the square marks indicate the secondary phase ( $\text{GdAlO}_3$ ).

The microstructures of the ceria powders were investigated using SEM, as seen in Fig. 2. As-prepared powders had near-spherical morphologies with an average size of  $\sim 0.95 \mu\text{m}$ . The spherical powders are the secondary particles consisting of primary nanoparticles. They were pelletized and then quickly sintered at  $1,400^\circ\text{C}$  using SPS (the relative densities of the green samples were in the range of 45–50%). After sintering, the relative densities of GDC and GDCAM, measured by the Archimedeian method, were  $\sim 94\%$  and  $96\%$ , respectively. The obtained densities were relatively high compared with the reported results prepared by conventional solid-state reaction [9]. In particular, GDCAM was highly sintered (note that this high density is reported to be achieved above  $1,500^\circ\text{C}$ ) [9]. The microstructure and element distribution of the sintered body of GDC and GDCAM were also investigated by SEM and EDS (the atomic percentages of Ce, Gd, Al and Mn were 78.4, 18.3, 1.9 and 1.4, respectively), and

high density and homogeneous element distribution were shown. Furthermore, the presence of this high density and secondary phase in GDCAM enhances the mechanical properties of ceria. The measured bending strength of GDC and GDCAM were  $\sim 90 \text{ MPa}$  and  $\sim 115 \text{ MPa}$ , respectively.

Electrical characteristics of GDC and GDCAM were investigated as follows. Fig. 3 shows their representative impedance data measured in air and reduced conditions (short term and long term), respectively. As seen in the figure, typical impedance spectra of conducting ceramics were observed. In Fig. 3(a), the spectrum consists of three parts corresponding to the grain, grain boundary (gb), and electrode, in that order, as indicated (note that the arcs corresponding to the grain and gb are almost semicircular, and the signals corresponding to the electrode are also imperfect arcs, but partially shown). Those parts are generated from the three respective resistances and capacitances ( $R_1C_1$ - $R_2C_2$ - $R_3C_3$ , series

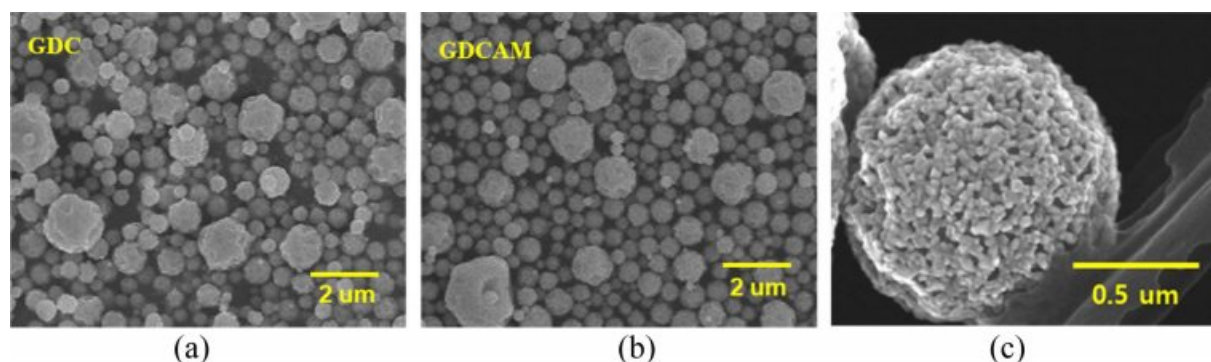


Fig. 2. FE-SEM images of as-prepared powders of (a) GDC and (b), (c) GDCAM.

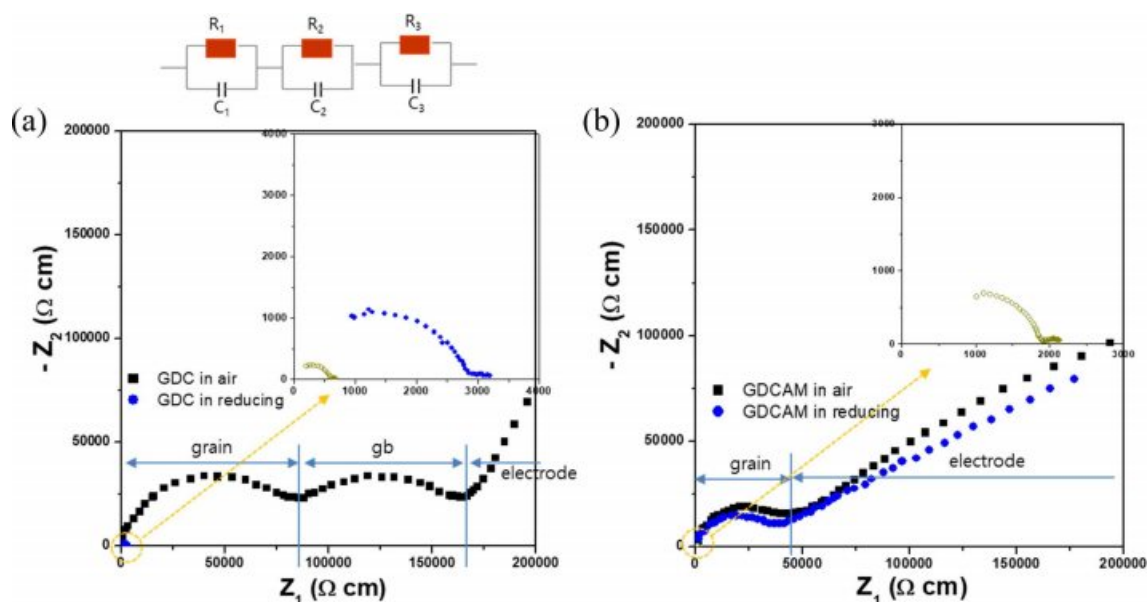


Fig. 3. The complex impedance plots of (a) GDC and (b) GDCAM at  $230^\circ\text{C}$ . Solid square symbols indicate the impedance patterns of GDC and GDCAM in air, and solid and open circles in the inset correspond those of GDC and GDCAM in reducing condition for short and long terms, respectively.

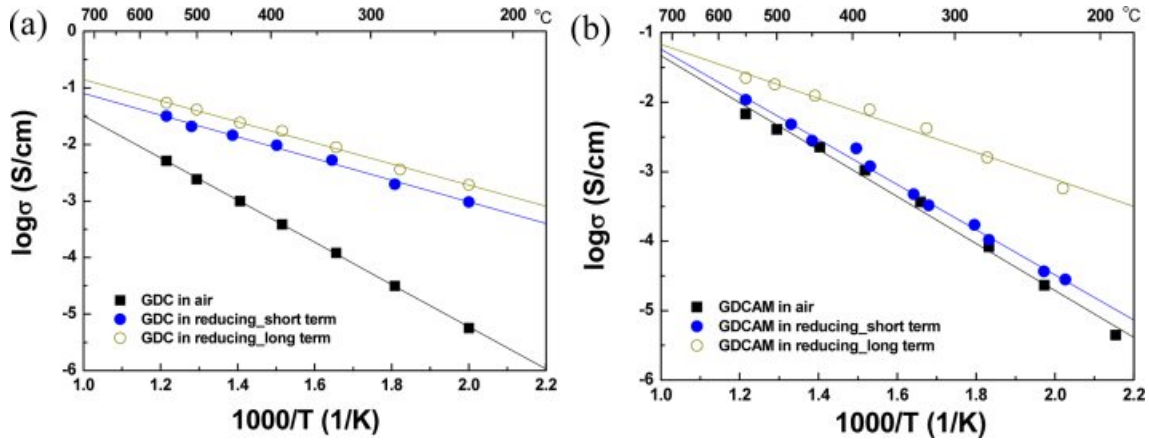


Fig. 4. Arrhenius plots of the total conductivities of (a) GDC and (b) GDCAM in various atmospheres.

equivalent circuit) of grain, gb and electrode. From the impedance patterns and equivalent circuits, the grain and gb resistances ( $R_{grain}$ ,  $R_{gb}$ ) were obtained ( $R_1C_1$  and  $R_2C_2$  were estimated for the grain and the gb by fitting the impedance spectrum using a corresponding equivalent circuit based on a bricklayer model:  $R_1 = R_{grain}$ ,  $R_2 = R_{gb}$ ). The total resistance of GDC, the summation of the grain and gb resistances, was also calculated. A notable point is that the arcs of the grain and gb of GDC became small in reduced condition, showing that the resistances of the grain and gb greatly decreased. When the sample was exposed in reduced condition for a long time, the arcs shrank further (the inset figure shows the pattern of GDC in reduced conditions). On the other hand, the pattern of GDCAM remained almost unchanged for a while, as shown in Fig. 3(b), even though it eventually shrank after long-time exposure (inset figure). Decreasing the size of the arc means less resistance, which is attributed to the generation of electronic conduction by  $Ce^{4+} \rightarrow Ce^{3+}$  under a reducing environment in ceria.

The temperature dependences of the total conductivities ( $s_{total} = 1/(R_{grain} + R_{gb}) \times L/A$ ,  $L$  and  $A$  being the length and area of the specimen) computed from the resistances are exhibited in Fig. 4(a) and (b). In this figure, the solid rectangular symbol represents the  $s_{total}$  of GDC in air. The activation energy ( $E_a$ ) is about 0.74 eV, indicating that the main charge carrier is the oxygen ion [18]. As expected from the impedance patterns, the  $s_{total}$  of GDC greatly increased in reduced conditions (solid blue symbol). After long-time exposure (open circle symbol), it increased further; on the other hand, in the short term,  $s_{total}$  (GDCAM) in the reducing environment was very similar to that in an air atmosphere (see Fig. 4b). This means that even in a reducing environment, ionic conduction is still a dominant charge carrier for the short term, and thus even in a reducing environment, the ionic transference number ( $t_i$ ) is near 1. However,  $s_{total}$  eventually greatly changed after long-time exposure in reducing conditions, showing

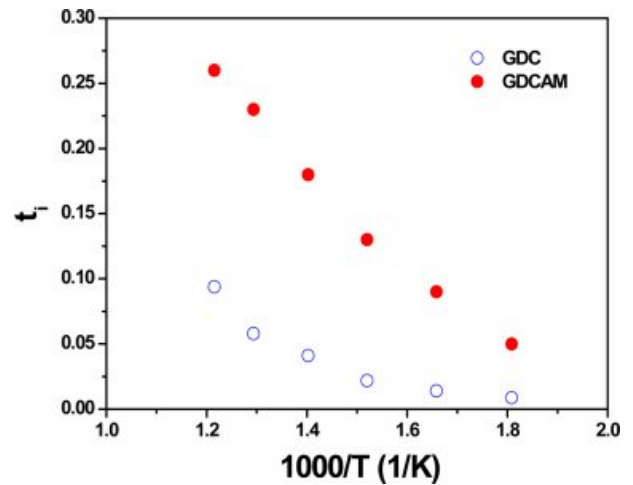
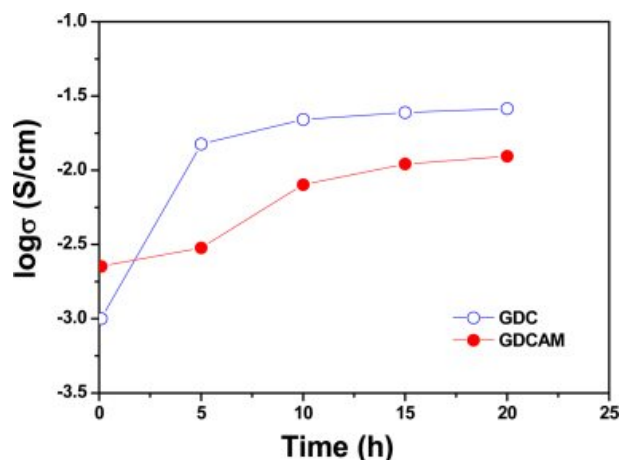


Fig. 5. Ionic transference numbers of GDC and GDCAM as a function of temperature.

that GDCAM can suppress the electronic conduction generated by cerium reduction ( $Ce^{4+} \rightarrow Ce^{3+}$ ) for a limited time. One interesting thing is that the  $s_{total}$  of GDCAM is still lower than the  $s_{total}$  of GDC, even though it is greatly changed after the long-term exposure. This means that the additives (Mn or Al) play a role in preventing cerium reduction.

Based on conductivity in air and in reducing atmosphere (long-time exposure),  $t_i$  was calculated and is shown in Fig. 5. As seen in the figure,  $t_i$  of GDCAM is higher than that of GDC, showing that GDCAM suppresses electron conduction in reducing conditions. This result demonstrates again that Al and Mn additions are effective in reducing Ce-reduction. Fig. 6 shows the time dependence of  $t_i$ s in GDC and GDCAM. The results confirm the suppression of the electronic conduction of GDCAM in reducing conditions.

As another effect of adding Al and Mn elements,  $s_{total}$  in air is increased compared to purely that of GDC, showing improved oxygen ionic conductivity (compare with  $s_{total}$ s of GDC (Fig. 4a) and GDCAM (Fig. 4b)).



**Fig. 6.** The total conductivities of GDC and GDCAM at 440 °C and in reducing condition as a function of time.

The  $s_{total}$  of GDCAM in air is also competitive or higher than the reported ionic conductivities. For example, the  $s_{total}$  of GDCAM at 500 °C is 0.004 S/cm and the reported values by S. Dikment et al. and H. Kim et al. are  $\sim 0.0009$  S/cm and 0.002 S/cm at the same temperature and oxygen partial pressure [9, 11]. It is believed that successfully synthesized nanoparticles using USP and multi-components (Al and Mn) increase the sinterability of ceria. The sample fabricated using conventional ceramic processing (solid-state reaction) shows a relative density below 95 % [9]. In this study, it was observed that increasing sinterability decreases grain and gb resistance (compare the gb resistances between Fig. 3a and b). The relative densities of GDC and GDCAM are  $\sim 94\%$  and  $96\%$ , respectively.

Conclusively, the addition of Al and Mn to ceria decreases total resistance, the summation of the grain and gb resistance, and more importantly, suppresses the electronic conduction in reducing atmosphere in ceria, demonstrating that it can be a viable solid electrolyte for IT-SOFC.

## Conclusions

In this study, Al- and Mn-added GDC was designed to overcome some weakness of a ceria solid electrolyte such as low sinterability and electronic conduction generation. GDC and Al- and Mn-added GDC powders were synthesized using USP and then sintered using spark plasma sintering technique. As a result, the successfully dense pellets were obtained. The addition

of Al and Mn components enhanced the relative density of the ceria leading to an increase of the ionic conduction and mechanical strength. More importantly, this addition suppressed the electronic conduction of ceria in reducing atmosphere, which is a major problem in the commercialization of ceria as a solid electrolyte for IT-SOFCs.

## Acknowledgments

I am very grateful to Prof. Y. Choa and Prof. H. Park for helping me synthesize powder and some experiments.

## References

1. B.C.H. Steele and A. Heinzl, *Nature* 414 (2001) 345-352.
2. N.Q. Minh, *J. Am. Ceram. Soc.* 76 (1993) 563-588.
3. T. Suzuki, Z. Hasan, Y. Funahashi, T. Yamaguchi, Y. Fujishiro and M. Awano, *Science* 325 (2009) 852-855.
4. Z. Shao and S.M. Haile, *Nature* 431 (2004) 170-173.
5. W. Zhou, R. Ran and Z. Shao, *J. Power Sources* 192 (2009) 231-246.
6. H.J. Park, T.G. Kim, C. Kwak, D.W. Jung, S.M. Lee and K.H. Lee, *J. Power Sources* 275 (2015) 884-887.
7. Z. Tianshu, P. Hing, H. Huang and J. Kilner, *Solid State Ionics* 148 (2002) 567-573.
8. J.G. Cheng, S.W. Zha, J. Huang, X.Q. Liu and G.Y. Meng, *Mater. Chem. and Phys.* 78 (2003) 791-795.
9. H.N. Kim, H.J. Park and G.M. Choi, *J. Electroceram.* 17 (2006) 793-795.
10. L. Ge, R. Li, S. He, H. Chen and L. Guo, *J. Power Sources* 230 (2013) 161-168.
11. S. Dikmen, P. Shuk, M. Greenblatt and H. Gocmez, *Solid State Sciences* 4 (2002) 585-590.
12. R.T. Leah, N.P. Brandon and P. Aguiar, *J. Power Sources* 145 (2005) 336-352.
13. S. Wang, T. Kobayashi, M. Dokiya and T. Hashimoto, *J. Electrochem. Soc.* 147 (2000) 3606-3609.
14. B. Wang, B. Zhu, S. Yun, W. Zhang, C. Xia, M. Afzal, Y. Cai, Y. Liu, Y. Wang and H. Wang, *NPG Asia Materials* 11 (2019) 51.
15. A. Arabaci and M.F. Oksuzomer, *Ceramics International* 38 (2012) 6509-6515.
16. D. Kashyap, P. K. Patro, R. K. Lenka, T. Mahata and P.K. Sinha, *Ceramics International* 40 (2014) 11869-11875.
17. H. J. Park and G.M. Choi, *Solid State Ionics* 178 (2008) 1746-1755.
18. J.D. Nicholas and L.C. De Jonghe, *Solid State Ionics* 178 (2007) 1187-1194.
19. Y.J. Kang and G.M. Choi, *Solid State Ionics* 180 (2009) 886-890.
20. Y.J. Kang, H.J. Park and G.M. Choi, *Solid State Ionics* 179 (2008) 1602-1605.